NASA Technical Memorandum 4515

Subsonic Aerodynamic Characteristics of the HL-20 Lifting-Body Configuration

George M. Ware and Christopher I. Cruz
Langley Research Center
Hampton, Virginia

National Aeronautics and Space Administration
Office of Management
Scientific and Technical Information Program
1993

Summary

A wind-tunnel investigation has been made in both the Langley 7- by 10-Foot High-Speed Tunnel and the Langley Low-Turbulence Pressure Tunnel to define the subsonic aerodynamic characteristics at a Mach number of 0.3 of a lifting-body configuration (the HL-20) proposed as a possible future manned spacecraft. The configuration has a low-aspect-ratio body with a flat undersurface. Three fins (a small centerline fin and two outboard (tip) fins set at a dihedral angle of 50°) are mounted on the aft body. The control system consists of elevon surfaces on the outboard fins, a set of four body flaps on the upper and lower aft body, and an all-movable center fin. The results of the study indicated that the model was longitudinally and laterally stable about an estimated center-of-gravity position at 54 percent of the body length. Both elevons and body flaps were capable of trimming the model to angles of attack from −2° to above 20°. The maximum trimmed lift-drag ratio was 3.6. Replacing the baseline flat-plate tip fins with airfoil tip fins increased the maximum trimmed lift-drag ratio to 4.2. The elevons were effective as a roll control, but they produced about as much yawing moment as rolling moment because of the tip-fin dihedral angle. The body flaps produced less rolling moment than the elevons and only small values of yawing moment. The tip-fin dihedral angle was varied from 90° to 0°. The baseline dihedral angle of 50° was determined to be a reasonable compromise for longitudinal and lateral stability, longitudinal trim, and performance at subsonic speeds.

Introduction

The National Aeronautics and Space Administration is investigating a number of configurations as possible manned spacecraft. Two of the current NASA mission studies are the Assured Crew Return Capability (ACRC) program (refs. 1 and 2) and the Personnel Launch System (PLS) program (refs. 3 to 7). The ACRC program provides for a safe emergency return to Earth for the Space Station *Freedom* crew. For this purpose, one or more return vehicles are docked at the Station ready for immediate use. The vehicles are to be carried to the Space Station in the 15- by 60-ft cargo bay of the Space Shuttle. The PLS, on the other hand, will be used to augment the Space Shuttle capabilities in the transportation of crew members to and from the Space Station. The PLS vehicle will be independently launched with an expendable booster and will return to Earth after exchanging crew members.

One of the candidate configurations under study for both the ACRC and the PLS programs is a lifting-body shape. The lifting body was chosen because it is volumetrically efficient and can generate lift to allow a low-deceleration atmospheric entry and horizontal landing. The configuration was designed to have moderate lift-drag values over the speed range. Moderate hypersonic lift-drag values give the vehicle a performance margin to deviate from its ballistic flight path to reach a suitable landing site or recovery area. At subsonic speeds, the lift-drag values should be sufficient for the vehicle to complete a conventional horizontal Shuttle-like landing. The lifting-body configuration of this investigation, designated the HL-20, consists of a low-aspect-ratio body with a flat undersurface and blunt base. Center and outboard fins are mounted on the upper aft body. The outboard fins are rolled outward from the vertical 40° (50° from the horizontal). Control surfaces are mounted on the outboard fins and aft body.

A series of wind-tunnel investigations has been undertaken to define the aerodynamic and aerothermodynamic characteristics of the HL-20 across the speed range from low-subsonic to hypersonic speeds (refs. 8–12). The present test was initiated to obtain additional subsonic aerodynamic information on the HL-20. Control effectiveness, Reynolds number effects, tip-fin dihedral effects, and tip-fin airfoil effects were studied. The resulting information was added to the aerodynamic data base for use in computer simulation of the vehicle flight behavior. The current tests were conducted in both the Langley 7- by 10-Foot High-Speed Tunnel (7 × 10 Tunnel) and the Langley Low-Turbulence Pressure Tunnel (LTPT) at a Mach number of 0.3. The Reynolds number, based on body length, ranged from 3.4×10^6 in the 7 × 10 Tunnel to 22.3×10^6 in the LTPT. The model was tested over a nominal angle-of-attack range of −2° to 30° at sideslip angles of 0° and 4°.

Symbols

The longitudinal data are referred to the stability-axis system and the lateral-directional data are referred to the body-axis system (fig. 1). All coefficients are based on the dimensions of the basic body without fins. The data are normalized by the planform area, length, and span of the body. The moment reference center was located at the vehicle center of gravity, which is at 54 percent of the body length from the nose and 0.08 percent of the body length above the flat lower surface.

b	body span, in.
C_D	drag coefficient, Drag/qS_{ref}
C_L	lift coefficient, Lift/qS_{ref}

C_l	rolling-moment coefficient, Rolling moment/$qS_{\text{ref}}b$
C_{l_β}	$= \Delta C_l/\Delta\beta$, taken at $\beta = 0°$ and $4°$, per degree
C_m	pitching-moment coefficient, Pitching moment/$qS_{\text{ref}}l$
C_n	yawing-moment coefficient, Yawing moment/$qS_{\text{ref}}b$
C_{n_β}	$= \Delta C_n/\Delta\beta$, taken at $\beta = 0°$ and $4°$, per degree
C_p	pressure coefficient, $(p_{\text{local}} - p_\infty)/q$
C_Y	side-force coefficient, Side force/qS_{ref}
C_{Y_β}	$= \Delta C_Y/\Delta\beta$, taken at $\beta = 0°$ and $4°$, per degree
c	chord
FS	fuselage station
L/D	lift-drag ratio
l	body length, in.
M	Mach number
p	pressure, lb/in^2
q	free-stream dynamic pressure, lb/in^2
R	Reynolds number
S_{ref}	basic body planform area (excluding fins), in^2
X	longitudinal body axis
Y	lateral body axis
x, y	coordinates of X and Y axes, respectively, of tip fins
Z	vertical body axis
α	angle of attack, deg
β	angle of sideslip, deg
Γ	tip-fin dihedral angle (measured from the horizontal), deg
Δ	increment
δ_a	aileron (differential pitch) control deflection angle, $(\delta_{e,L} - \delta_{e,R})/2$ or $(\delta_{\text{BF},L} - \delta_{\text{BF},R})/2$, deg
δ_{BF}	body-flap deflection angle (positive when deflected downward), deg
δ_e	elevon deflection angle (positive when deflected downward), deg
δ_r	rudder deflection angle (positive when trailing edge deflected left), deg

Subscripts:

basic	baseline configuration (no control deflections)
L	left
max	maximum
R	right
trim	trimmed condition (zero moment)
∞	free stream

Description of Model

Sketches of the model are presented in figure 2, and a photograph is presented in figure 3. Model dimensional information is given in table I. The aluminum model was a 0.059-scale representation of a 29.15-ft-long vehicle. The configuration consisted of a low-aspect-ratio body with a flat undersurface and a blunt base. Three fins were mounted on the upper aft portion of the model. The centerline fin was relatively small, and the larger outboard fins were set at a dihedral angle of 50°, a toe-in angle of 1.25°, and an incidence angle at the body intersection of 6.6°. The baseline fins had a thick flat-plate cross section with a cylindrical leading edge and blunt trailing edge (fig. 2(e)).

Control surfaces, referred to as "elevons," made up the trailing edges of the outboard fins. In addition, the model had four body-flap control surfaces, two on the upper body and two on the lower body. Their surfaces were flush with the body contour and could only be deflected outward. For positive body-flap deflection, the lower body flap was deflected downward while the upper body flap remained undeflected. For negative body deflection, the upper body flap was deflected upward while the lower body flap remained undeflected. During the current test, only the left elevon or left upper or lower body flap was deflected. Control deflections of 0°, −10°, 10°, −20°, 20°, −30°, and 30° were tested. The dihedral angle of the outboard fins was varied by replacing the original ($\Gamma = 50°$) fins with those having dihedral angles of 0°, 25°, 75°, and 90°.

An alternate set of outboard tip fins with an airfoil cross section was tested. The airfoil tip fin is shown in figure 2(e) and has a slightly different planform from that of the flat-plate fin, but it retained the dihedral angle, toe-in angle, and incidence angle of the baseline. The airfoil fins were 8-percent thick at the root and 12-percent thick at the tip. The airfoil coordinates are presented in table II. A speed

brake configuration was investigated that simulated aft-body side-mounted panels hinged at the forward end and deflected 45°.

Apparatus, Test, and Corrections

Tests were conducted in both the 7 × 10 Tunnel and the LTPT. The 7 × 10 Tunnel is a subsonic closed-circuit wind tunnel with a nominal 7- by 10-ft test section. Because tests are conducted at atmospheric pressure, Reynolds number varies with Mach number. The facility is capable of test Mach numbers up to 0.9. The LTPT is a low-subsonic pressure tunnel with a 3-ft-wide by 7.5-ft-high test section. It is capable of pressures up to 10 atm that give it a Reynolds number range per foot from 2×10^6 to 15×10^6.

In both tunnels, the model was sting mounted through its base, and forces and moments were measured with an internally mounted strain gauge balance. Model angles of attack and sideslip were corrected for sting and balance deflection under load. Customary tunnel interference corrections were applied to the data. In an attempt to ensure turbulent flow over the model in the 7 × 10 Tunnel, transition grit was applied in accordance with reference 13 and as shown in figure 4. The No. 150 grit was thinly sprinkled in 1/16-in. bands 1.2 in. aft of the nose and 0.3 in. perpendicular to the leading edges of the fins. In addition, 1/16-in. bands of grit were added along the lower body radius. Transition grit was not used in the LTPT. Instead, an initial test was made to determine the Reynolds number at which the changes in aerodynamic characteristics ceased. The remaining tests were conducted at or above this Reynolds number.

The model test pitch range was nominally from −2° to 20°. The model was tested at angles of sideslip of 0° and 4° over the angle-of-attack range. Data were taken as the model was moved from negative to positive angles. Model base and cavity pressures were measured and are presented as figure 5 in the event that base corrections are desired.

Results and Discussion

Because the aerodynamic data generated in this investigation were to be used in a computer-driven flight simulation program, the data were taken in a form that would readily adapt to that program. The simulator information, which takes the form of the basic aerodynamic parameters for a configuration with controls undeflected, forms other conditions by adding increments due to control deflections. (Other increments due to aerodynamic damping, ground effects, aeroelastic effects, etc., may also be added.) From this information, the vehicle control matrix for the flight envelope is described. Therefore, during the wind-tunnel test, only a single control surface was deflected during a run. (In this case, the left elevon or body flap was deflected.) The resulting incremental change in the aerodynamic parameters was used with the baseline aerodynamics to make up the characteristics of the vehicle with multiple control surfaces deflected. For example, pitch control for an elevon deflection of −20° is made up of the baseline aerodynamic characteristics plus twice the aerodynamic increments produced by a deflection of −20° of the left elevon alone.

The direct addition of increments may introduce errors if the interference effects of one control on the other are not considered. Fortunately, the elevons and body flaps of the lifting-body model are physically separated by a distance that tends to minimize interference. Presented in figure 6 is a comparison of the aerodynamic characteristics of the model with both elevons deflected −10° and characteristics of the model with a single elevon deflected −10° and its effects doubled. The data are taken from a test in the Calspan 8-Foot Transonic Tunnel of the HL-20 model (ref. 8). Incremental elevon effects from the current investigation were added to the characteristics of the model with $\delta_e = 0°$ from the Calspan test. The two sets of data are in good agreement.

The aerodynamic characteristics of the lifting-body model with controls deflected, presented in the following figures with brief comments, were determined by adding increments as previously described. The equations are

$$C_L = C_{L,\text{basic}} + \Delta C_{L,\delta e} + \Delta C_{L,\delta\text{BF}}$$
$$C_D = C_{D,\text{basic}} + \Delta C_{D,\delta e} + \Delta C_{D,\delta\text{BF}}$$
$$C_m = C_{m,\text{basic}} + \Delta C_{m,\delta e} + \Delta C_{m,\delta\text{BF}}$$
$$L/D = C_L/C_D$$

Longitudinal Characteristics

Basic aerodynamics and pitch control. The longitudinal aerodynamic characteristics of the lifting-body model with elevons deflected as a pitch control are presented in figures 7 and 8. Data are taken from tests in the 7 × 10 Tunnel at a Mach number of 0.3 for control deflections ranging from −30° to 30°. The model is trimmed with controls undeflected at an angle of attack of about 10°. At this angle of attack (and Reynolds number), the lift-drag ratio is 3.4, which is approximately $(L/D)_{\max}$. A

positive elevon deflection of 30° trimmed the model to approximately $\alpha = -2°$, where lift and L/D were negative. Full negative elevon deflection trimmed the HL-20 to an angle of attack of 23° (extrapolated), which is well above the maximum lift-drag value and proposed landing attitude.

The pitch-control effectiveness of the body flaps (fig. 8) is about the same as that of the elevons in this speed range. A body-flap deflection of 30° to −30° trimmed the model from −2° to over 20°. Some nonlinearity in pitching-moment effectiveness occurred at body-flap settings of −20° and −30°. It is speculated that with increasing Reynolds number, the flow will remain attached over the body at the flaps and the variation will become more linear. The control power of either elevons or body flaps is sufficient to trim the HL-20 over the envisioned subsonic flight envelope.

Tip-fin dihedral effects. The effect of varying the tip-fin dihedral angle from 90° to 0° is presented in figure 9. These data from the 7 × 10 Tunnel show that fin rotation, as expected, has a major effect on the longitudinal characteristics of the HL-20. At $\Gamma = 90°$, the model is unstable and untrimmed over the test range. At $\Gamma = 0°$, it is highly stable and trimmed at an angle of attack of 8°. Maximum untrimmed lift-drag ratio varies from 3.9 to 2.7. The model is untrimmed in the nominal operational angle-of-attack range at fin dihedral angles of 75° and above. Positioning the fins at $\Gamma = 50°$ appears to be an acceptable compromise for trim and performance (L/D) in this speed range.

Speed brake effects. During gliding flight to landing, adjusting the flight path to reach the desired site may become necessary. For this purpose, the model was fitted and tested with body-mounted speed brakes. (See fig. 2(a).) The results of these tests with brakes closed and open at 45° are presented in figure 10. The rather large speed brakes (9 percent of the body reference area) were very effective in increasing drag and resulted in an increase in longitudinal stability. A 5° negative shift in longitudinal trim, however, also occurred. This adverse effect on trim indicates that a coordinated pitch-control input must accompany deflection of the speed brakes. Other means of modulating drag, such as the simultaneous deflection of all four body flaps, may be a better alternative than the deflection of the body-mounted speed brakes.

Reynolds number effects. The Reynolds number effects were studied in the LTPT. Figure 11 shows the effect of increasing the Reynolds number from 3.4×10^6 to 22.3×10^6 (based on body length) on the aerodynamic characteristics of the HL-20 configuration. Increasing the Reynolds number causes little change in lift or pitching moment, but sufficient change in drag occurs to increase L/D from 3.2 to 3.6. A full-scale flight Reynolds number based on a 29-ft-long vehicle is approximately 60×10^6 at a landing speed of 200 knots. Note that above a test Reynolds number of 10.3×10^6, the longitudinal parameters remain relatively constant, a result suggesting that data taken at the higher Reynolds numbers of the LTPT test reflect full-scale vehicle performance characteristics.

Effect of tip-fin airfoil shape. In an attempt to improve the subsonic performance of the HL-20, additional tests were conducted in the LTPT in which the flat-plate tip fins were replaced by airfoil tip fins. (See fig. 2(e) and table II.) The effect of the fin change is shown in figure 12. Increasing the model lift and reducing the drag resulted in an increase in $(L/D)_{max}$ to 4.3. The changes in lift and drag caused an increase in longitudinal stability and a shift in longitudinal trim from about 10° to 7°. The characteristics of the airfoil-fin HL-20 configuration trimmed over an angle-of-attack range with body-flap deflection (increments taken from fig. 8) are given in figure 13. The data indicate a trimmed $(L/D)_{max}$ of approximately 4.2, an improvement of 0.6 over that of the model with flat-plate fins.

Lateral Characteristics

Lateral-directional stability. The lateral-directional characteristics of the HL-20 are presented in figure 14 in the form of the stability parameters C_{Y_β}, C_{n_β}, and C_{l_β} plotted against angle of attack. Data are shown for the baseline HL-20 (flat-plate tip fins with $\Gamma = 50°$) and for fins at $\Gamma = 90°$, 75°, 25°, and 0°. The baseline HL-20 ($\Gamma = 50°$) is directionally stable, has positive values of C_{n_β} over the angle-of-attack range, and has positive effective dihedral (negative values of C_{l_β}). Increasing the tip-fin dihedral angle from 50° to 90° increased the aft lateral plane area of the configuration and increased directional stability, as would be expected. With tip-fin dihedral angle set at 25°, the model had neutral directional stability, and at $\Gamma = 0°$ it was unstable. All configurations had positive effective dihedral. Therefore, if static directional stability is to be maintained, tip-fin dihedral angle must be greater than 25°. The baseline tip-fin dihedral angle of 50° (which was shown to be a reasonable compromise in the longitudinal plane) appears satisfactory from the lateral-directional standpoint.

Roll-control effects. All lateral-control tests were made with the baseline configuration. Roll control was accomplished through differentially deflecting the elevons on the outboard fins or the body flaps on the upper aft body. Only negative control deflections (upward deflections) are shown. The effectiveness values are for cases in which the left upper elevon or left body flap was set at $-10°$, $-20°$, and $-30°$ while the right control remained at $0°$. These deflections represent $-5°$, $-10°$, and $-15°$ of roll control deflection about a pitch setting of $-5°$, $-10°$, and $-15°$, respectively.

Roll effectiveness data are presented in figure 15(a) for the elevons and in figure 15(b) for the body flaps. The elevons, with their longer transverse moment arm, were much more effective in producing rolling moment than the body flaps. The simultaneous deflection of elevons and body flaps was not tested, and whether their effectiveness values are directly additive is unknown. Differential deflection of the elevons as a roll control produced about as much adverse yawing moment (ΔC_n) as favorable rolling moment (ΔC_l) because of the rolled-out fin configuration. Differential deflection of the elevons caused them to act as much like a rudder as like ailerons. The yawing moment associated with body-flap deflection, on the other hand, was favorable and much smaller. If the elevons are used for roll control, a control device such as a rudder may be needed to offset the yawing moments produced.

Yaw-control effects. Yaw control is accomplished by pivoting the small center fin about its midchord. Rudder effectiveness tests were conducted in the Calspan 8-Foot Transonic Tunnel and are reported in reference 8. Although these tests were made at $M = 0.6$, the characteristics are felt to be about the same as those at $M = 0.3$. The data from the Calspan test are repeated in figure 16. The values presented are for data taken at fin deflection angles of $0°$ and $5°$. The yaw effectiveness is essentially constant over the angle-of-attack range. The all-movable center fin produced only small cross-coupled moment, that is, small values of adverse rolling moment. The effectiveness of the center fin as a yaw control, however, was low.

Concluding Remarks

An investigation has been made in both the Langley 7- by 10-Foot High-Speed Tunnel and the Langley Low-Turbulence Pressure Tunnel to define the subsonic aerodynamic characteristics of the HL-20 lifting-body configuration at a Mach number of 0.3. The results indicated that the model was longitudinally stable and had a maximum trimmed lift-drag ratio of 3.6. Elevons located on the outboard fins or body flaps on the aft body were capable of trimming the model over the proposed subsonic operational angle-of-attack range. The trimmed lift-drag ratio was increased to 4.2 when the baseline flat-plate tip fins were replaced with airfoil tip fins. The elevons were effective as a roll control, but they produced about as much yawing moment as rolling moment because of the tip-fin dihedral angle. Differential body-flap deflection resulted in lower values of rolling moment but produced little yawing moment. The yawing moment from deflection of the center fin was constant over the angle-of-attack range with little associated rolling moment. The effectiveness of the center fin, however, was low. A limited investigation of the effect of tip-fin dihedral angle for the HL-20 indicated that the original-design dihedral angle of $50°$ was a reasonable compromise for longitudinal and lateral stability, longitudinal trim, and performance at subsonic speeds.

NASA Langley Research Center
Hampton, VA 23681-0001
September 8, 1993

References

1. Ware, George M.; Spencer, Bernard, Jr.; and Micol, John R.: Aerodynamic Characteristics of Proposed Assured Crew Return Capability (ACRC) Configuration. AIAA 89-2172, July/Aug. 1989.

2. Hook, W. Ray; and Freeman, Delma C., Jr.: Lifting-Body Option for a Space Station Rescue Vehicle. IAF Paper 89-246, Oct. 1989.

3. Naftel, J. Chris; Powell, Richard W.; and Talay, Theodore A.: Performance Assessment of a Space Station Rescue and Personnel/Logistics Vehicle. *J. Spacecr. & Rockets*, vol. 27, no. 1, Jan.–Feb. 1990, pp. 76 81.

4. Piland, William M.; Talay, Theodore A.; and Stone, Howard W.: Personnel Launch System Definition. IAF-90-160, Oct. 1990.

5. Talay, Theodore A.; and Stone, Howard W.: The Personnel Launch System A Lifting Body Approach. IAF Paper 91-202, Oct. 1991.

6. Stone, Howard W.; and Piland, William M.: The HL-20 Lifting-Body Personnel Launch System. SAE Paper 911970, Oct. 1991.

7. Talay, Theodore A.: The HL-20 Personnel Launch System. AIAA-92-1416, Mar. 1992.

8. Ware, George M.: *Transonic Aerodynamic Characteristics of a Proposed Assured Crew Return Capability (ACRC) Lifting-Body Configuration.* NASA TM-4117, 1989.

9. Ware, George M.: *Supersonic Aerodynamic Characteristics of a Proposed Assured Crew Return Capability (ACRC) Lifting-Body Configuration.* NASA TM-4136, 1989.

10. Cruz, Christopher I.; Ware, George M.; Grafton, Sue B.; Woods, William C.; and Young, James C.: *Aerodynamic Characteristics of a Proposed Personnel Launch System (PLS) Lifting-Body Configuration at Mach Numbers From 0.05 to 20.3.* NASA TM-101641, 1989.

11. Micol, John R.: Experimental and Predicted Aerodynamic Characteristics of a Proposed Assured Crew Return Vehicle (ACRV) Lifting-Body Configuration at Mach 6 and 10. AIAA-90-1403, June 1990.

12. Horvath, Thomas J.; Rhode, Matthew N.; and Buck, Gregory M.; Acrothermodynamic Measurements on a Proposed Assured Crew Return Vehicle (ACRV) Lifting-Body Configuration at Mach 6 and 10 in Air. AIAA-90-1744, June 1990.

13. Braslow, Albert L.; Hicks, Raymond M.; and Harris, Roy V., Jr.: Use of Grit-Type Boundary-Layer-Transition Trips. *Conference on Aircraft Aerodynamics*, NASA SP-124, 1966, pp. 19 36.

Table I. Geometric Characteristics of Model

Body alone:	
Aspect ratio	0.6
Length (reference length), in.	20.6
Span (reference span), in.	9.7
Planform area (reference area), in^2	152.2
Base area (excluding cavity area), in^2	23.2
Cavity area, in^2	4.9
Height (maximum), in.	4.7
Body with fins ($\Gamma = 50°$):	
Aspect ratio	1.5
Length (body), in.	20.6
Span (outboard fins tip to tip), in.	16.3
Planform area, in^2	178.6
Base area (no cavity and fin base area), in^2	23.2
Cavity area, in^2	4.9
Height (to tip of outboard fin), in.	5.9
Elevons:	
Chord, in.	1.1
Span, in.	4.1
Thickness, in.	0.4
Area (each), in^2	3.5
Body flaps:	
Chord, in.	1.5
Span, in.	2.3
Area (each), in^2	3.5
Speed brakes:	
Area (each), in^2	6.8

Table II. Airfoil Tip-Fin Coordinates

	Root chord		Tip chord	
x/c	Upper y/c	Lower y/c	Upper y/c	Lower y/c
0	0	0	0	0
.10	.0565	↓	.0848	↓
.20	.0705		.1058	
.30	.0777		.1165	
.40	.0800		.1200	
.50	.0777		.1165	
.60	.0709		.1064	
.70	.0573		.0896	
.80	.0443		.0664	
.90	.0249		.0373	
1.00	.0050		.0050	

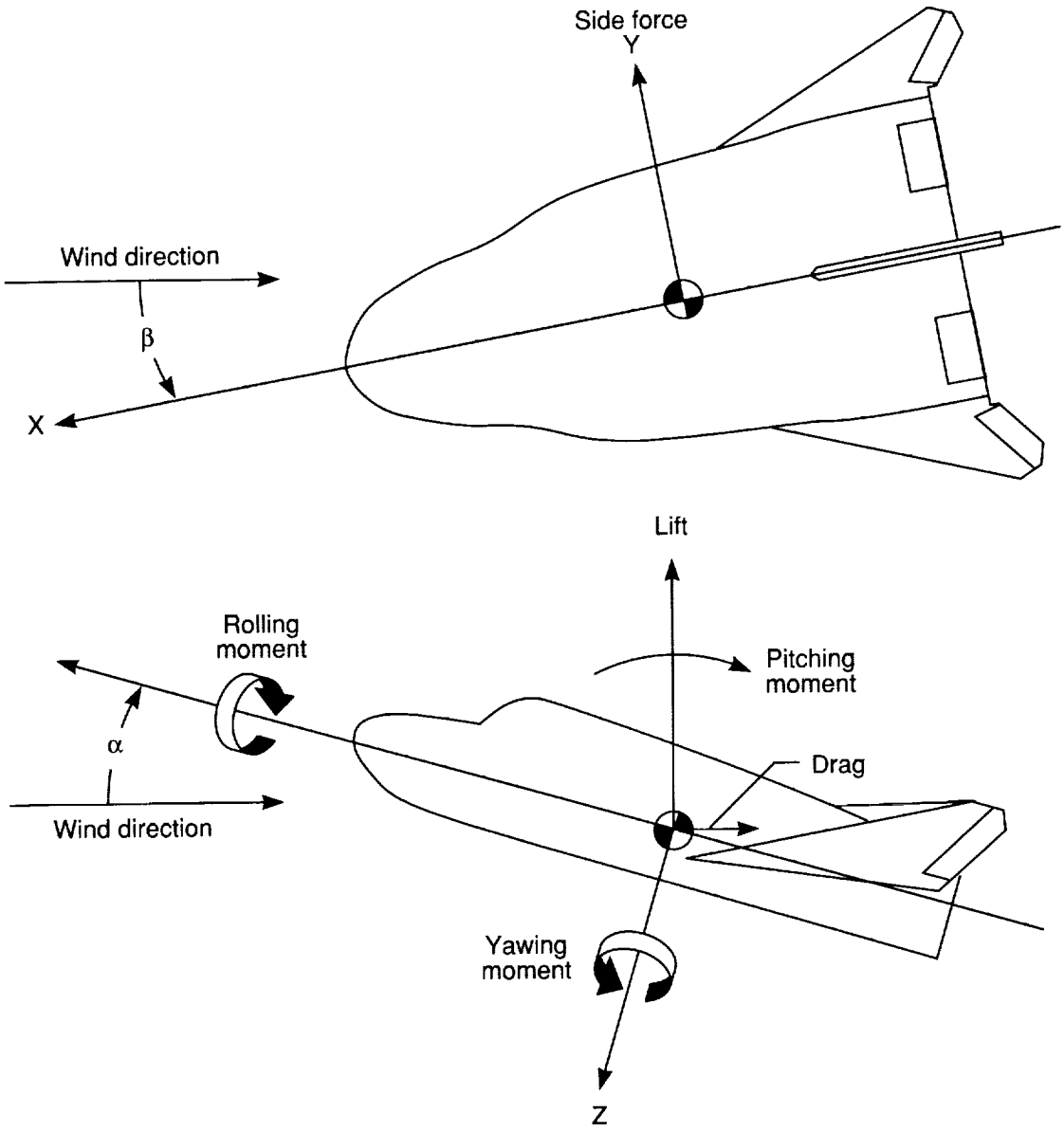

Figure 1. Sketches of axis systems used in investigation.

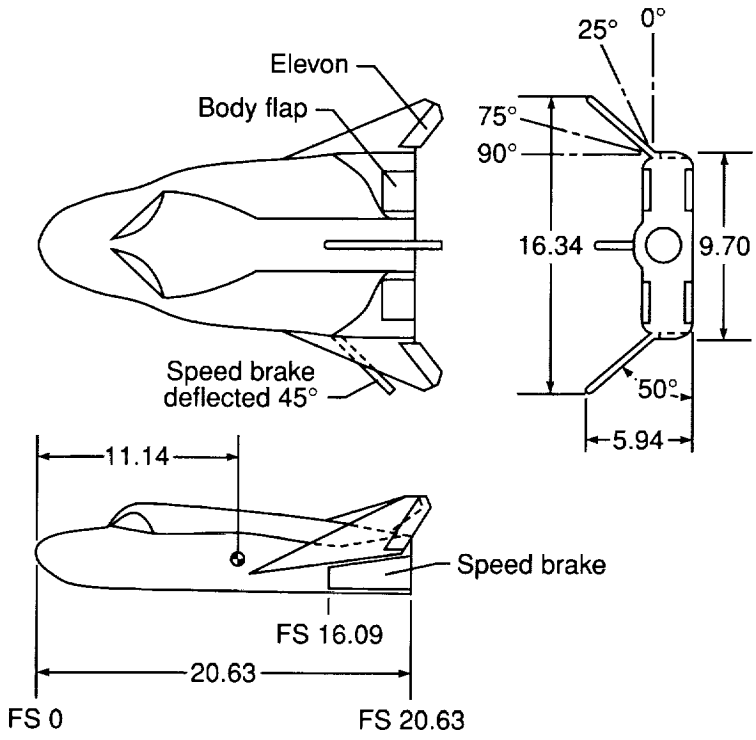

(a) General arrangement.

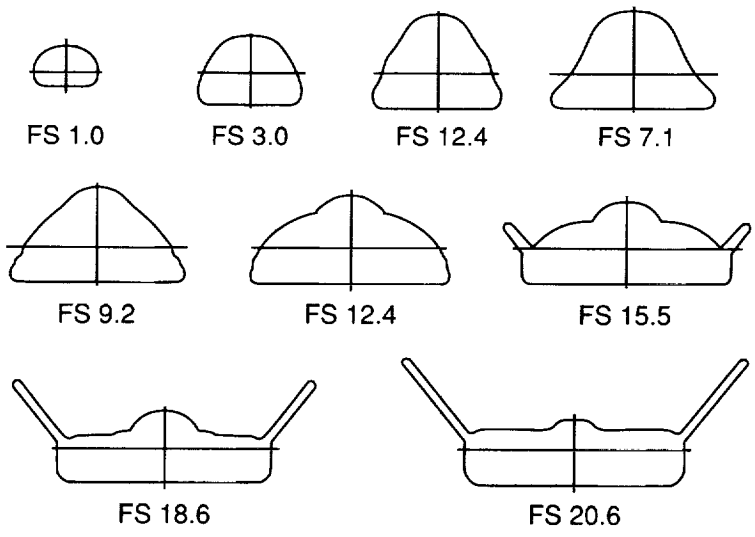

(b) Body cross sections.

Figure 2. Sketches of HL-20 model used in investigation. All dimensions are given in inches.

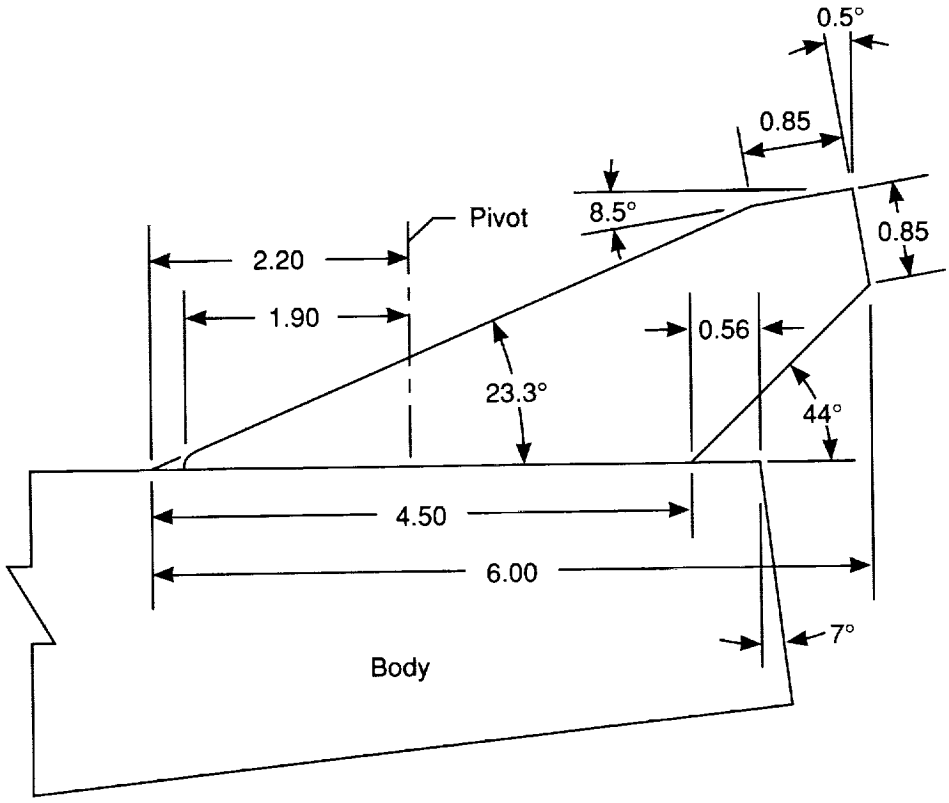

(c) Center-fin details.

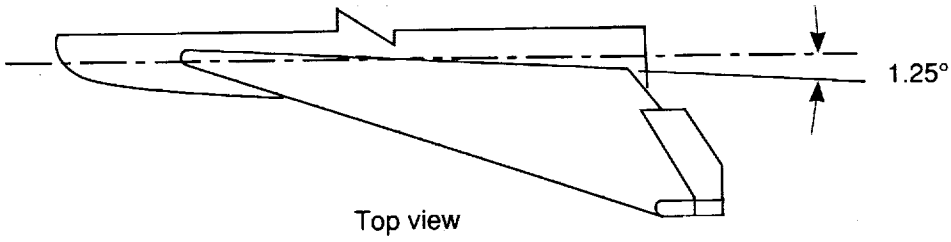

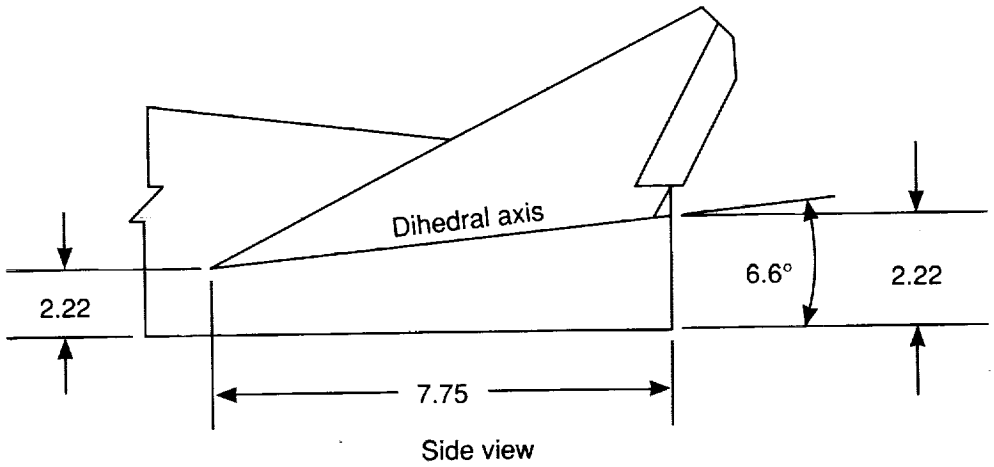

(d) Tip incidence and toe-in angles.

Figure 2. Continued.

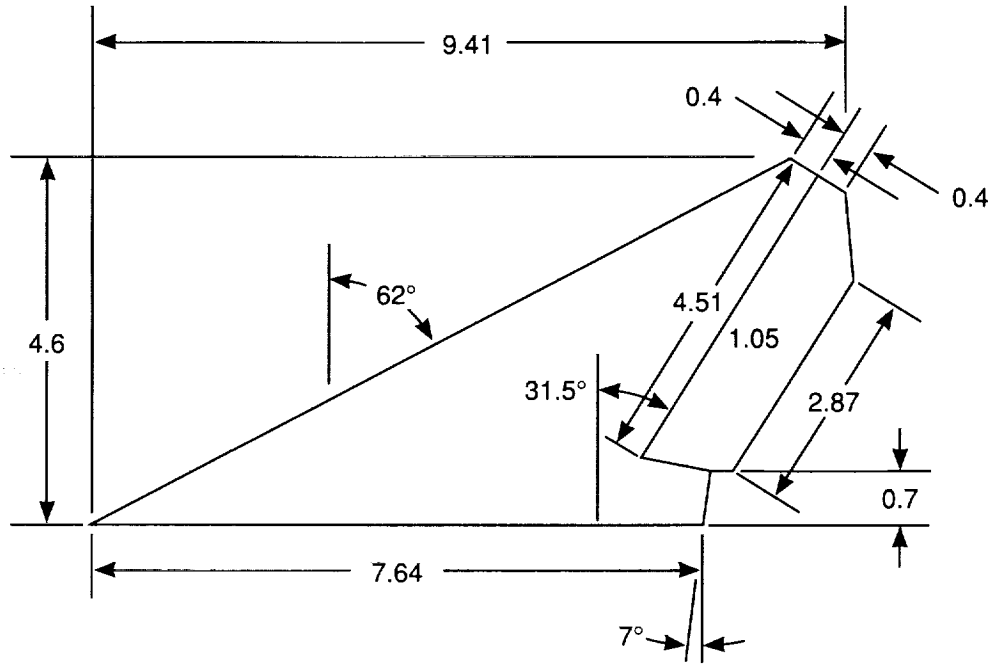

Flat-plate tip-fin details

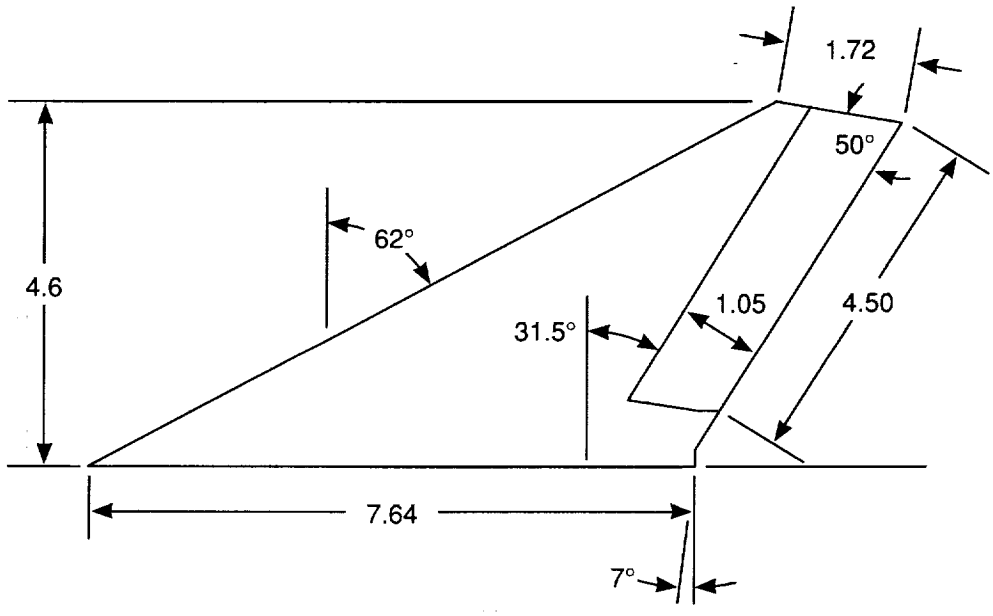

Airfoil tip-fin details

(e) Tip-fin details. Measurements are made in plane of fin.

Figure 2. Concluded.

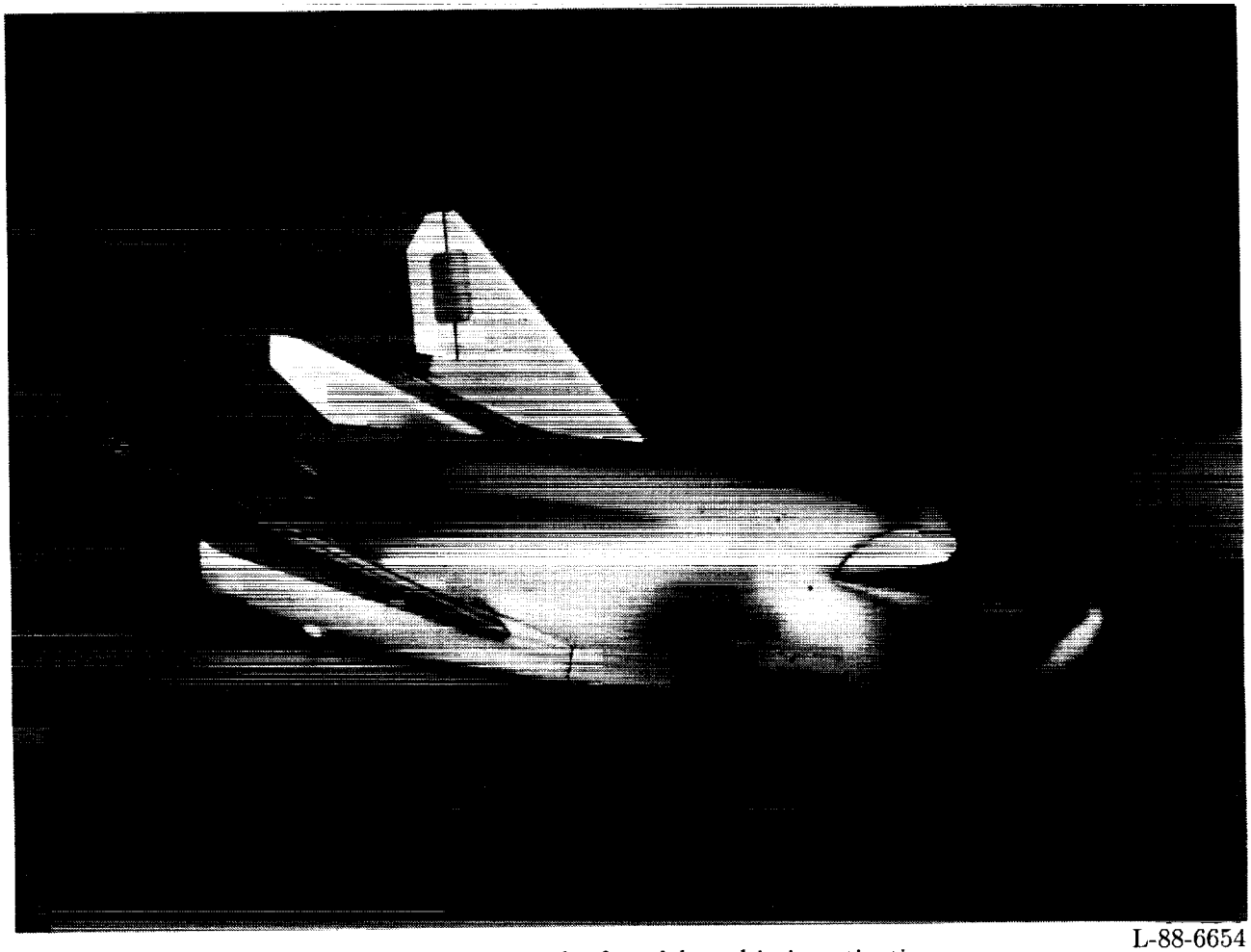

L-88-6654

Figure 3. Photograph of model used in investigation.

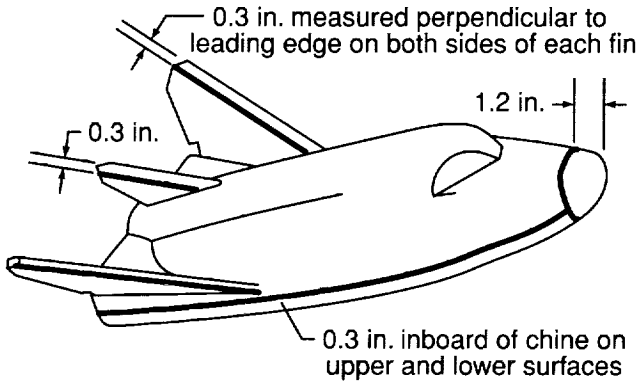

Figure 4. Sketch of model showing transition grit locations (shaded areas). No. 150 size grit was used.

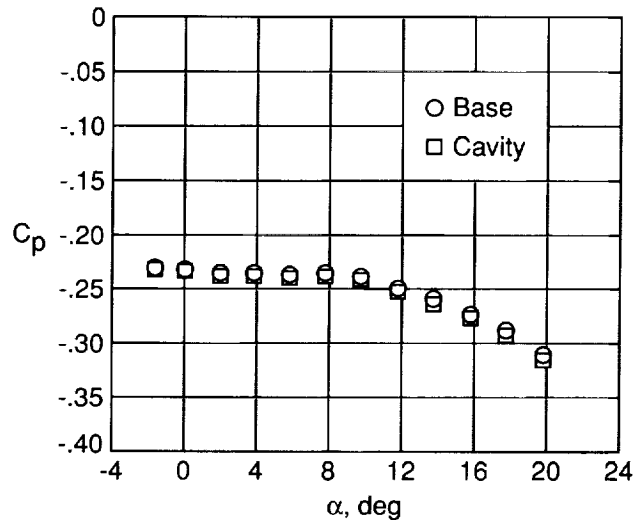

Figure 5. Pressure coefficient values of base and cavity.

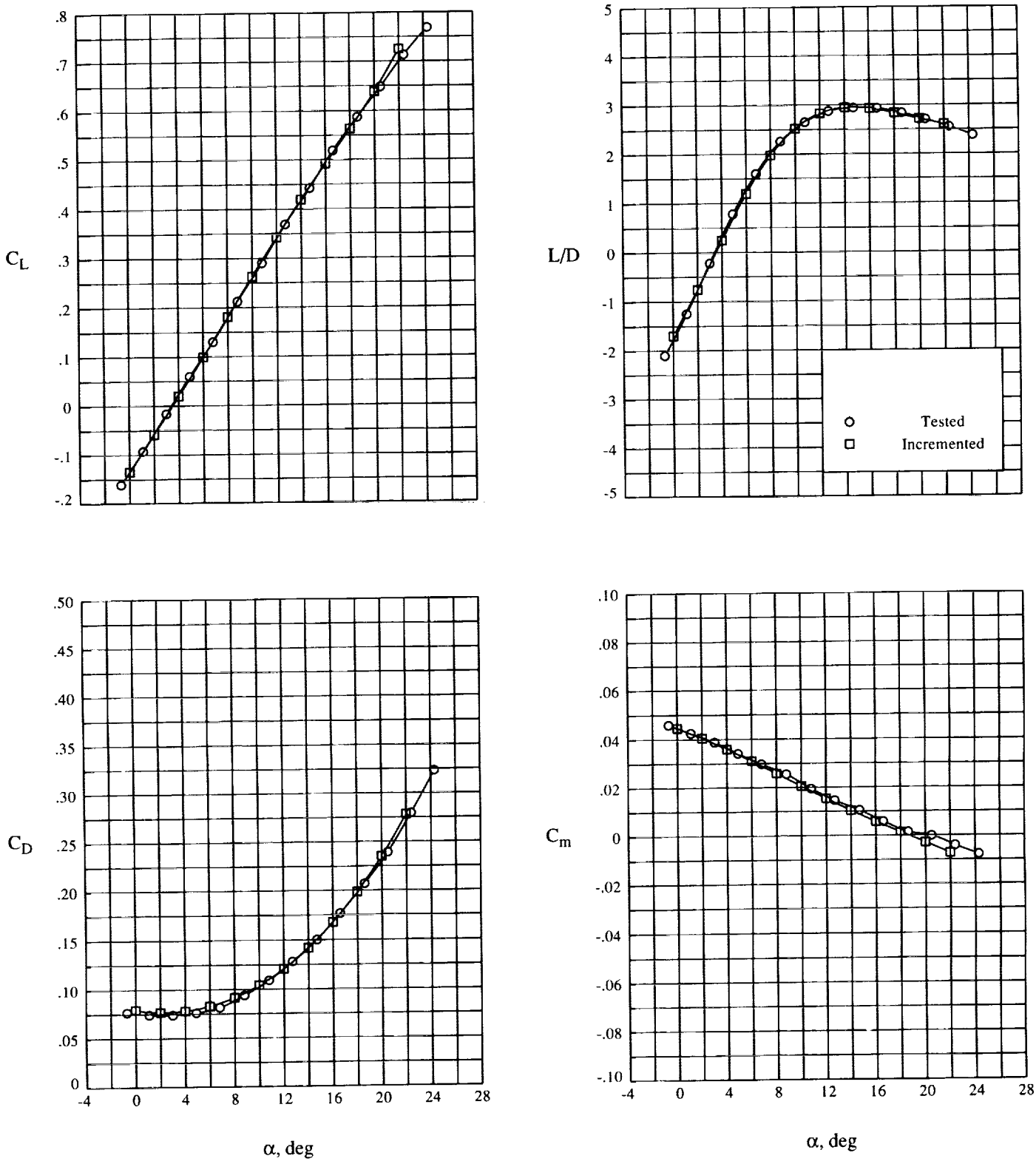

Figure 6. Comparison of tested and incremented longitudinal aerodynamic characteristics at $M = 0.6$ and $\delta_e = -10°$. Data are taken from reference 8.

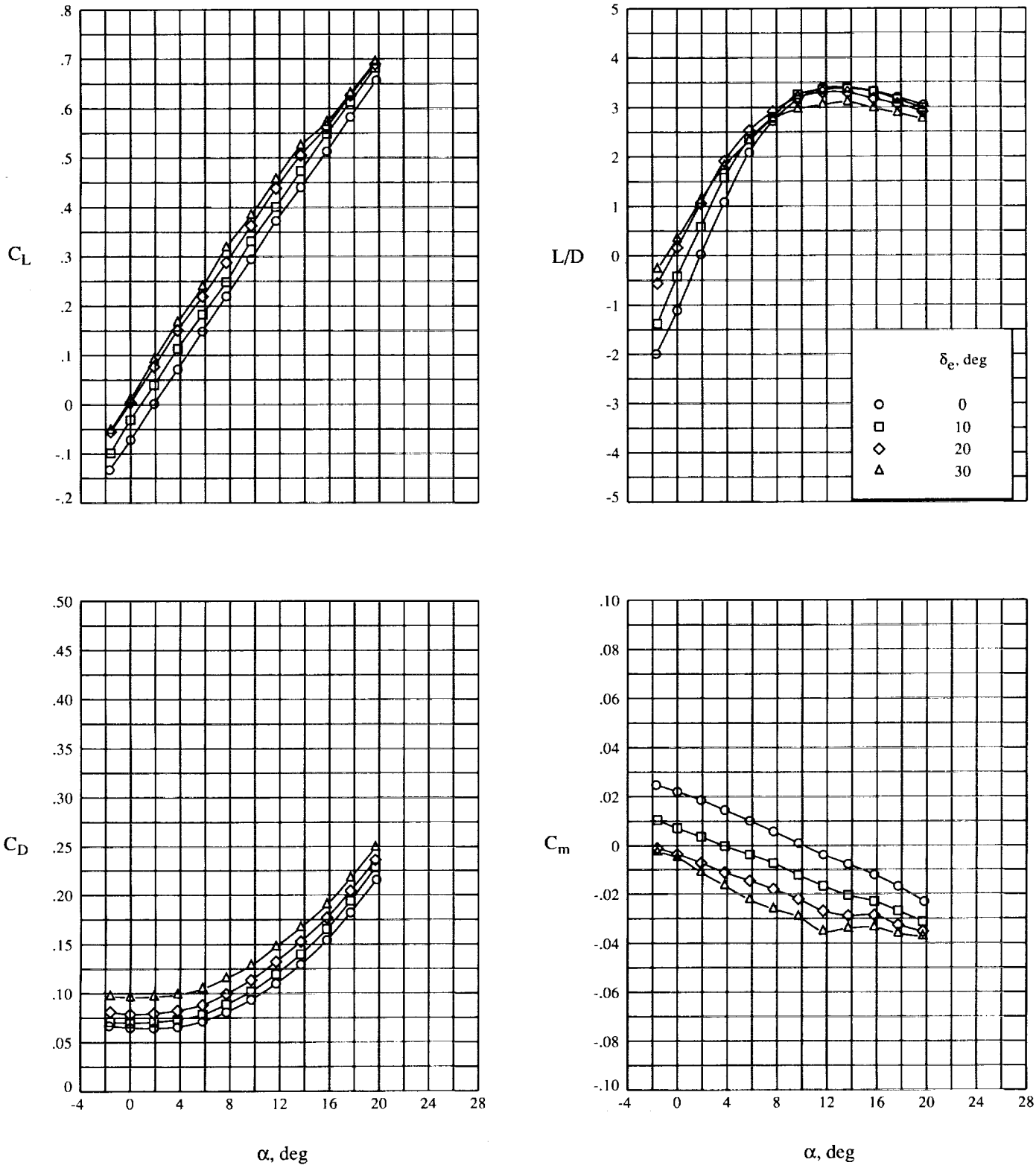

(a) Positive deflection.

Figure 7. Effect of elevon deflection on longitudinal aerodynamic characteristics.

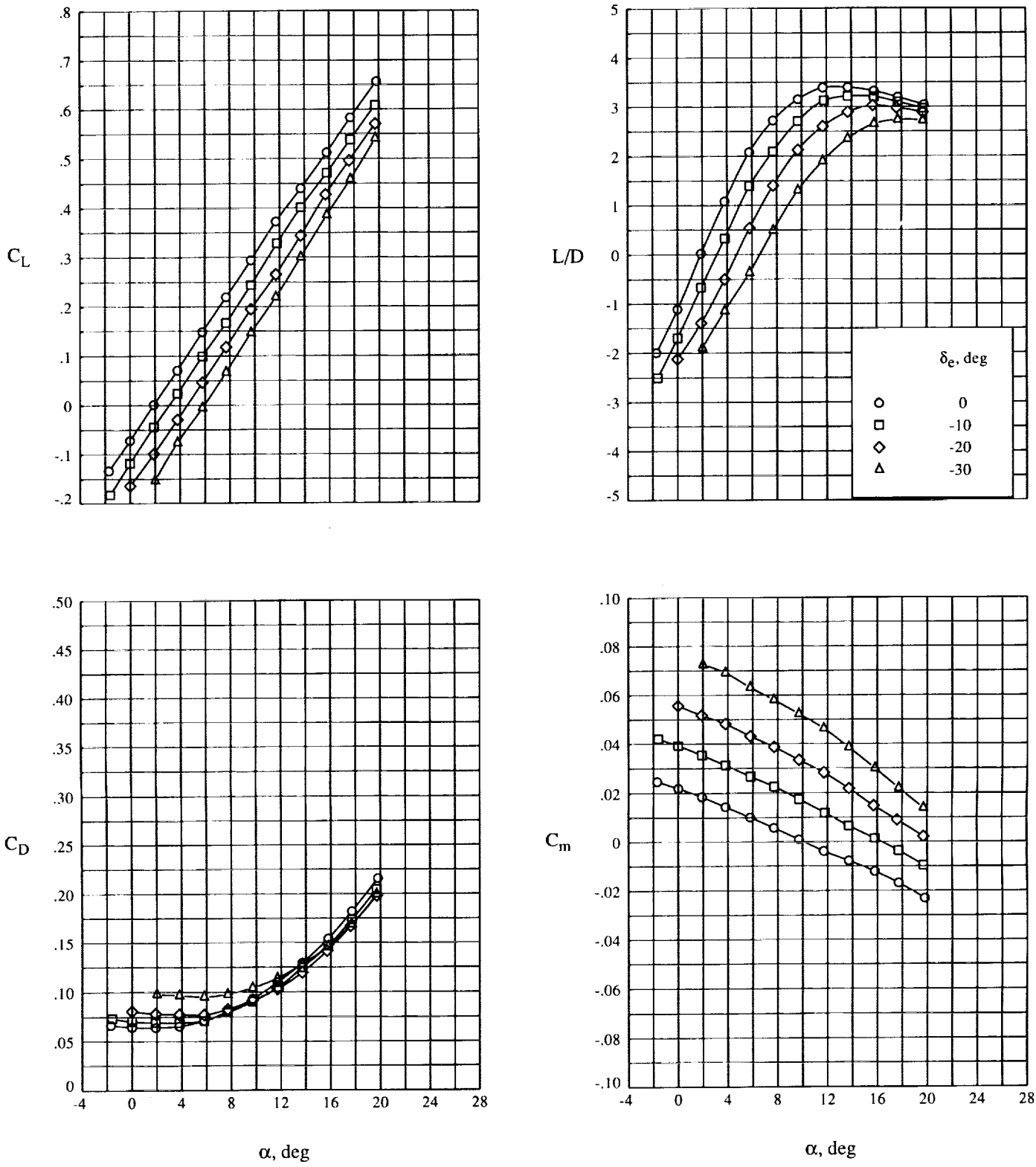

(b) Negative deflection.

Figure 7. Concluded.

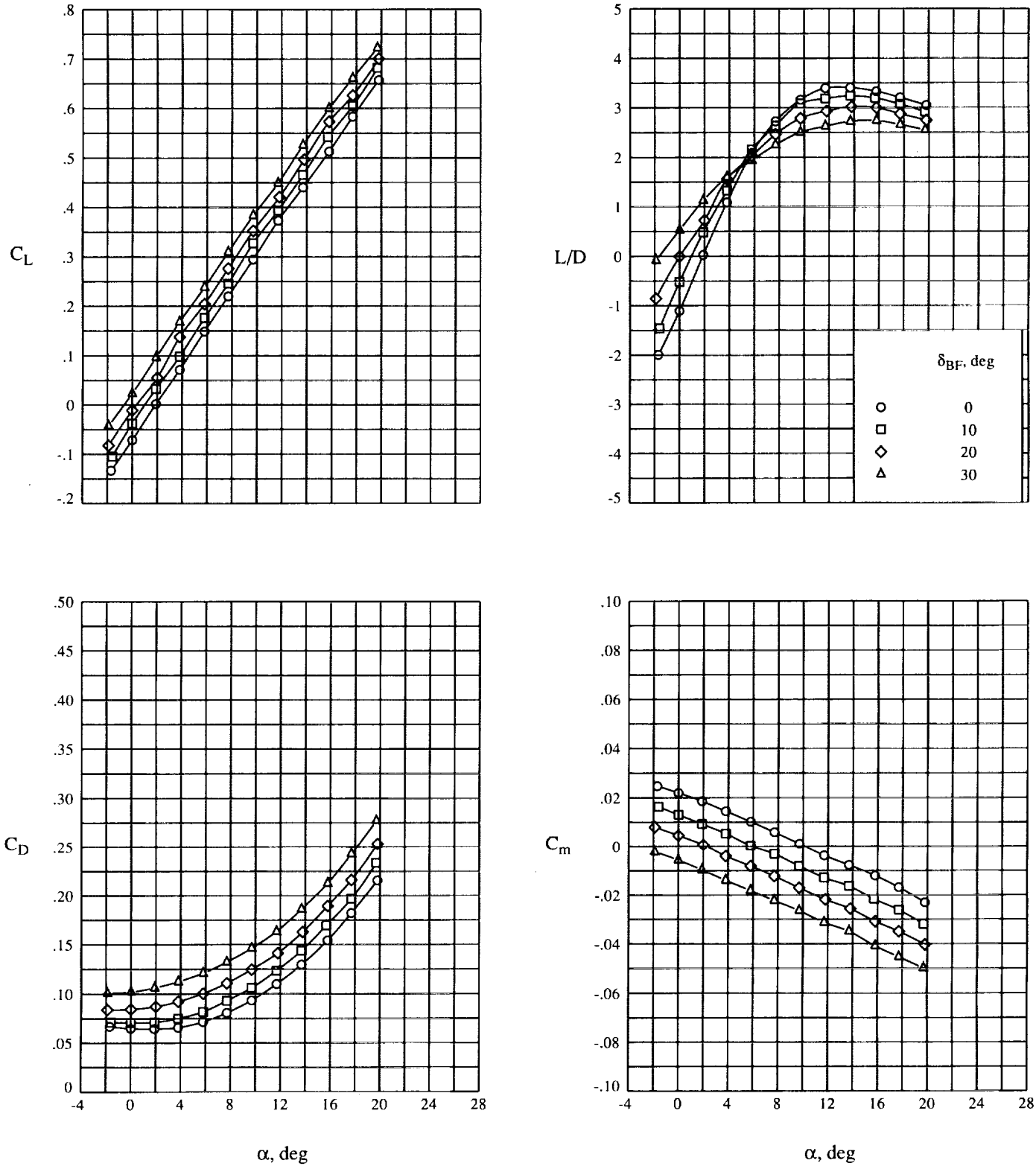

(a) Positive deflection.

Figure 8. Effect of body-flap deflection on longitudinal aerodynamic characteristics.

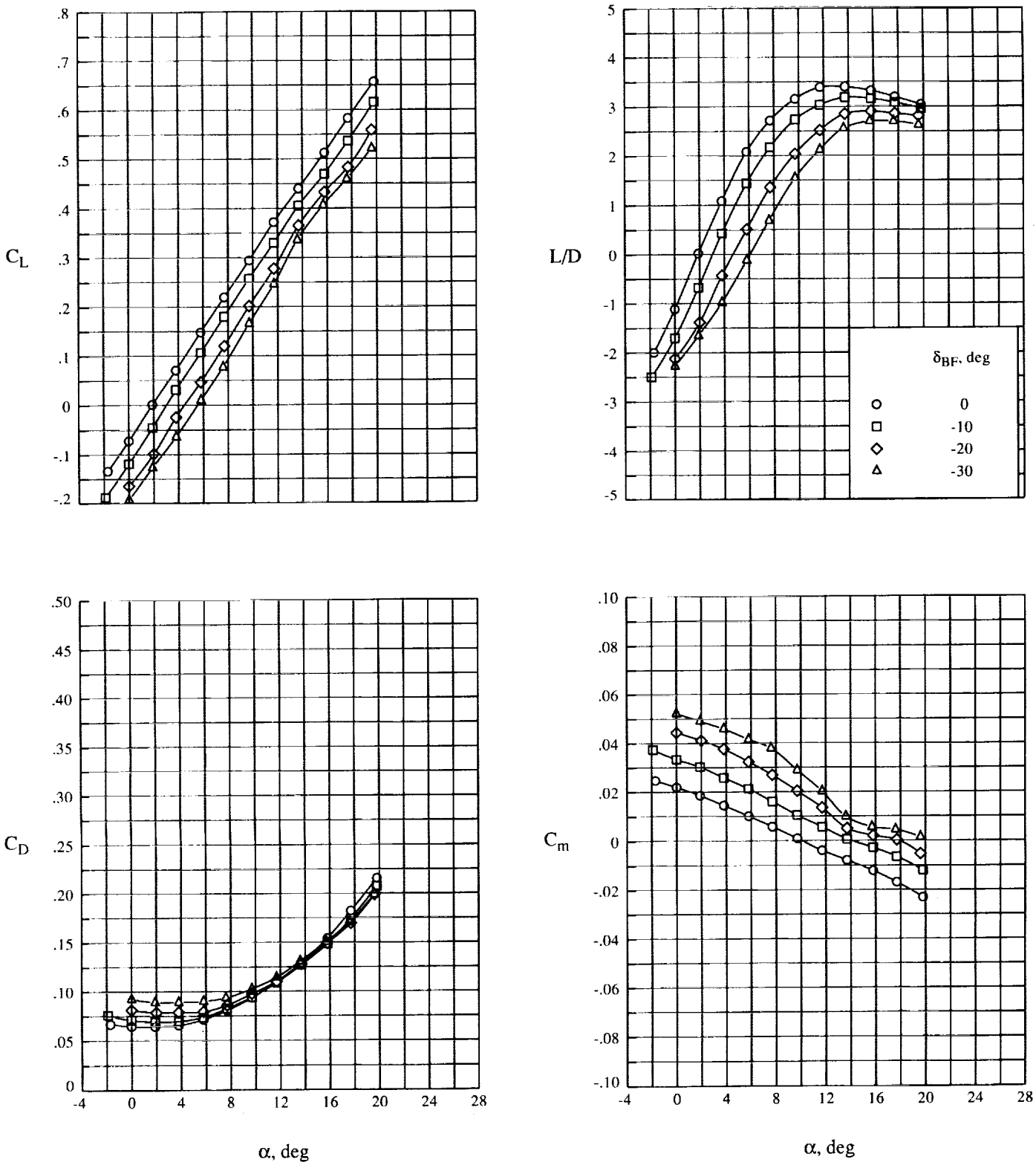

(b) Negative deflection.

Figure 8. Concluded.

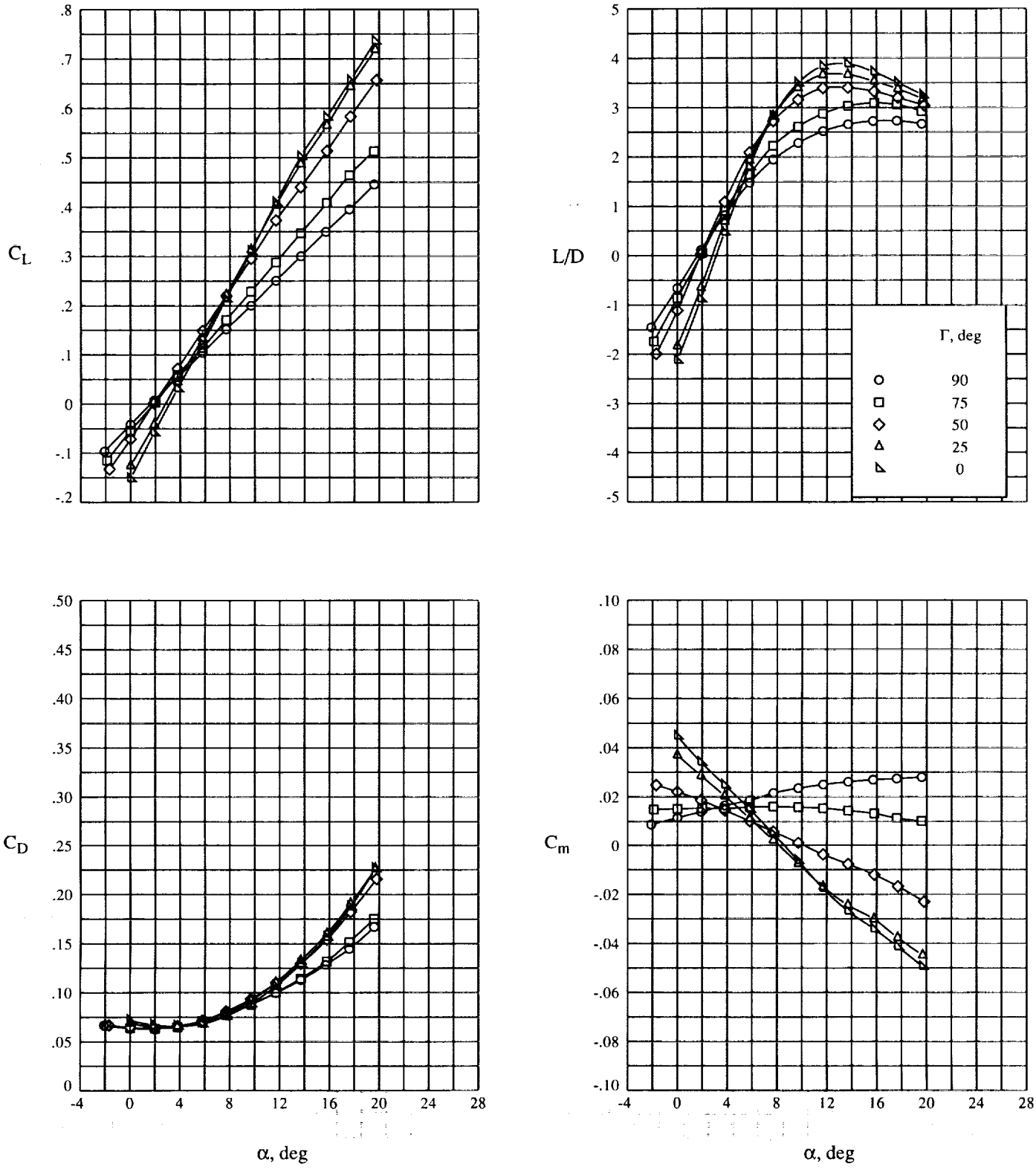

Figure 9. Effect of tip-fin dihedral angle on longitudinal aerodynamic characteristics.

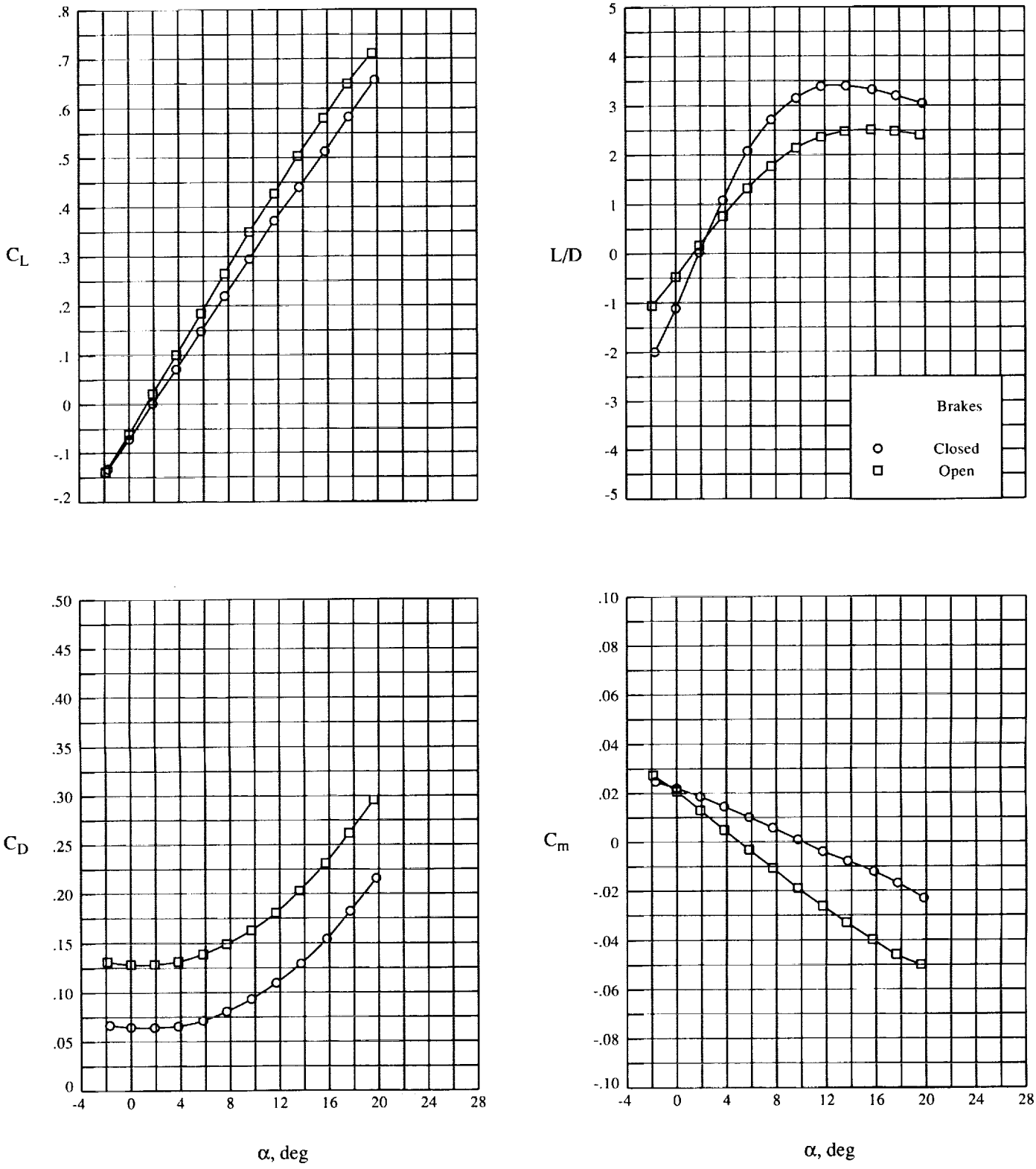

Figure 10. Effect of body-mounted speed brakes on longitudinal aerodynamic characteristics.

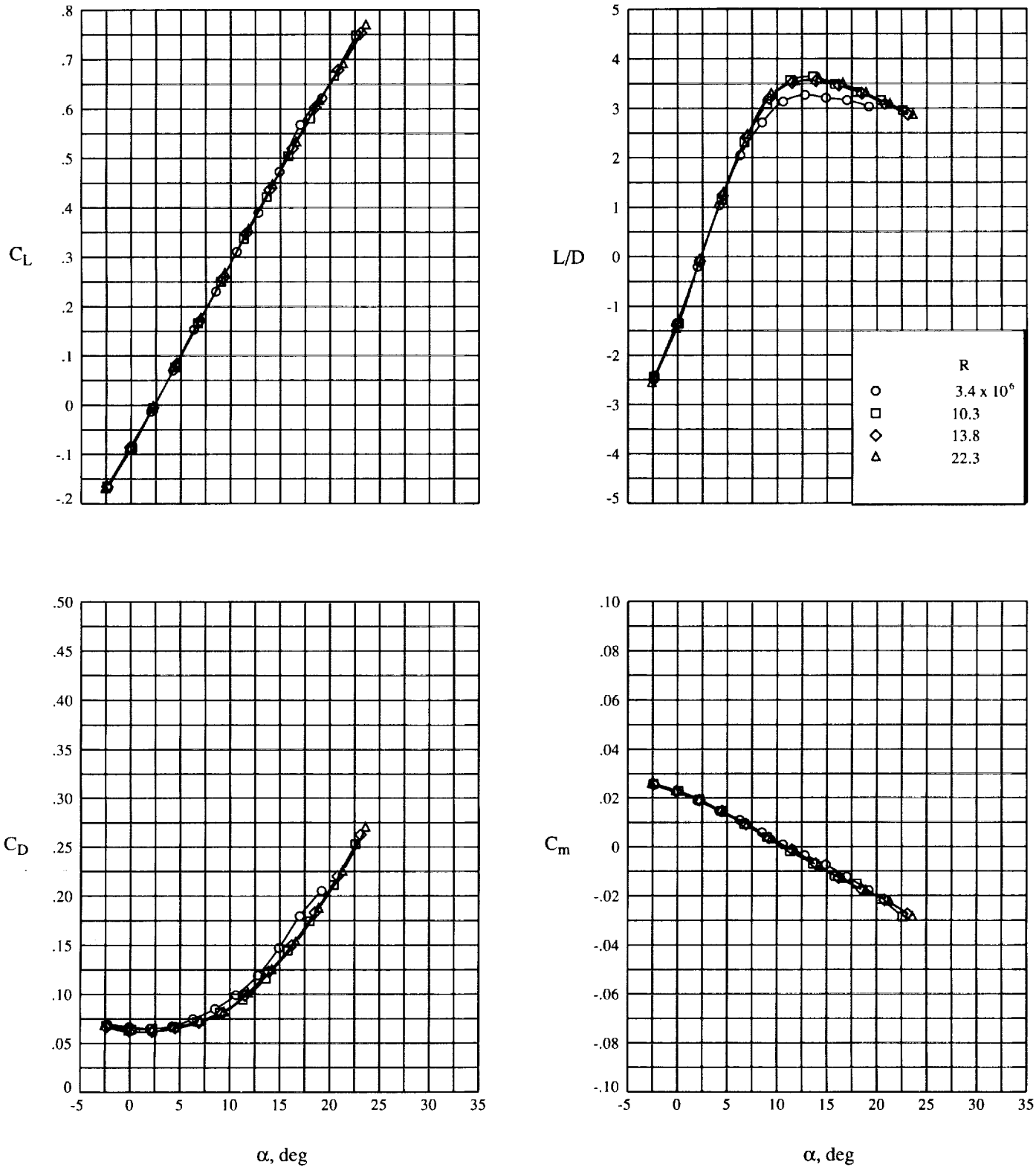

Figure 11. Effect of Reynolds number on longitudinal aerodynamic characteristics.

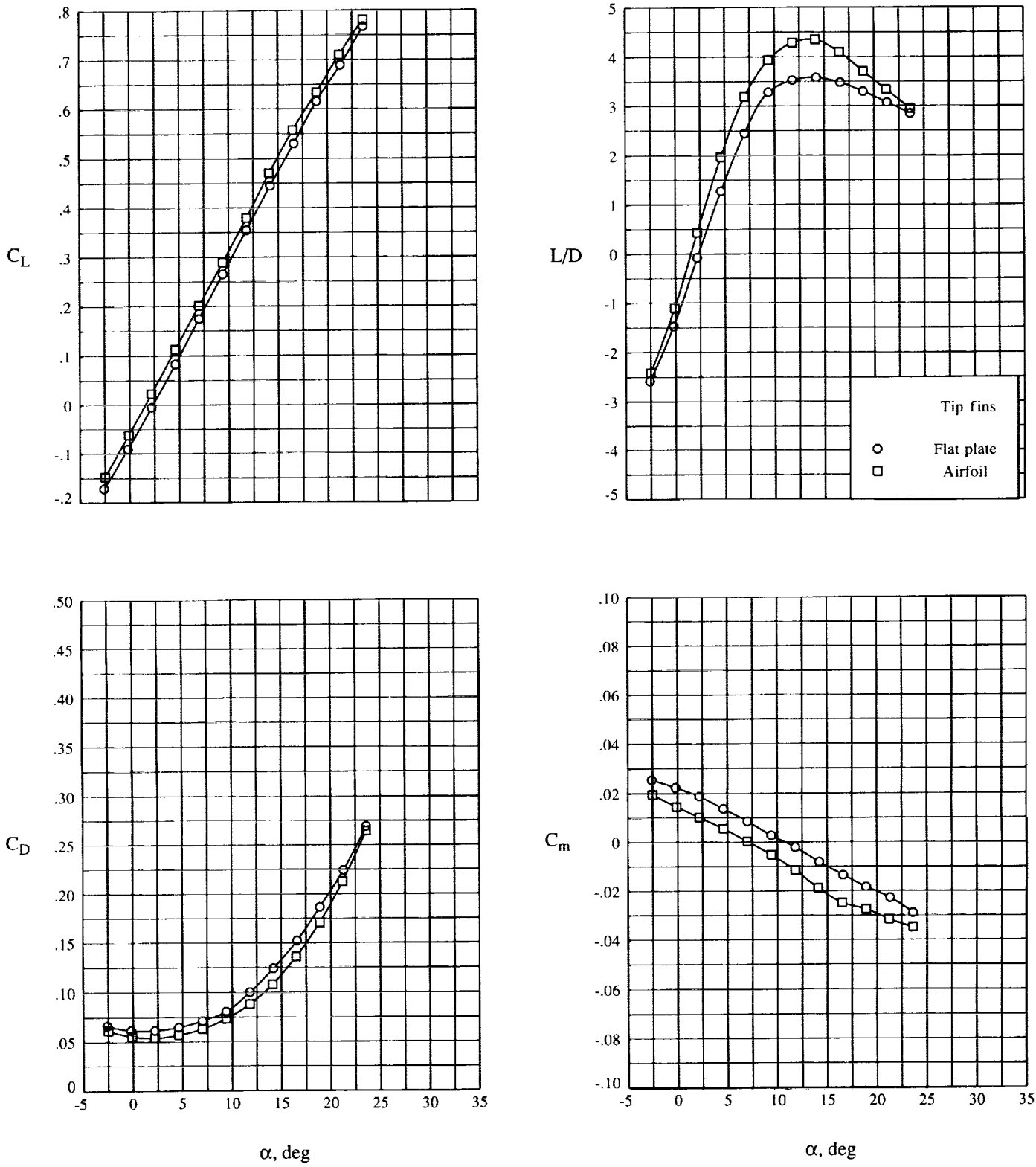

Figure 12. Effect of tip-fin cross section on longitudinal aerodynamic characteristics at $R = 22.3 \times 10^6$.

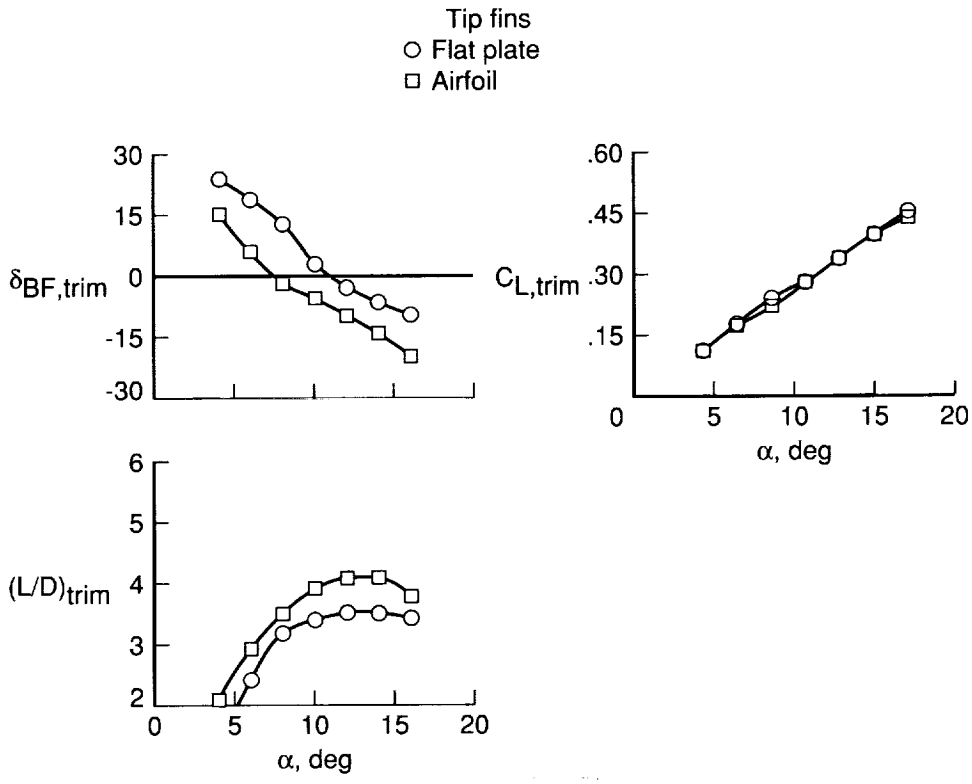

Figure 13. Longitudinal trim characteristics.

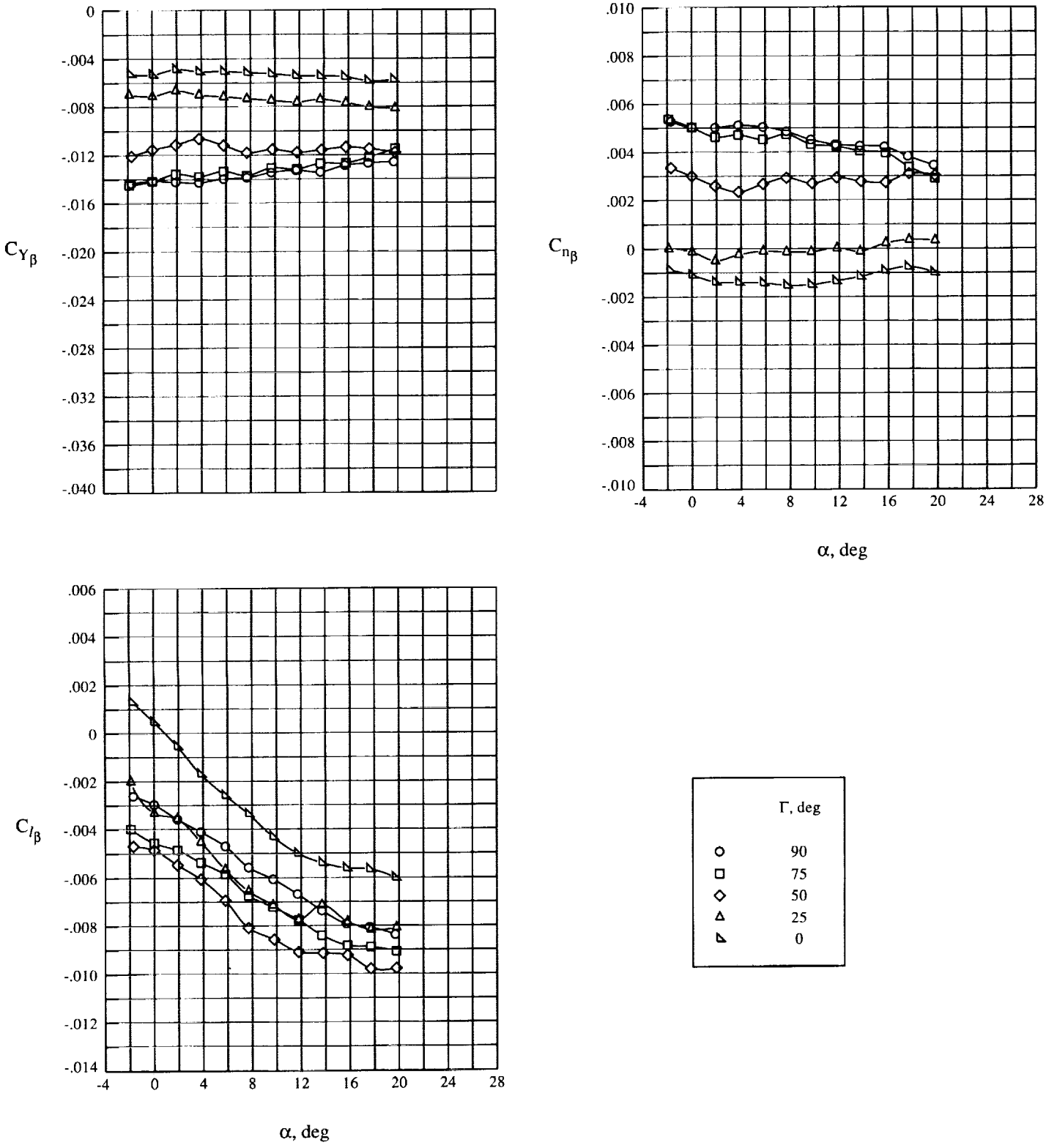

Figure 14. Effect of tip-fin dihedral angle on lateral stability characteristics.

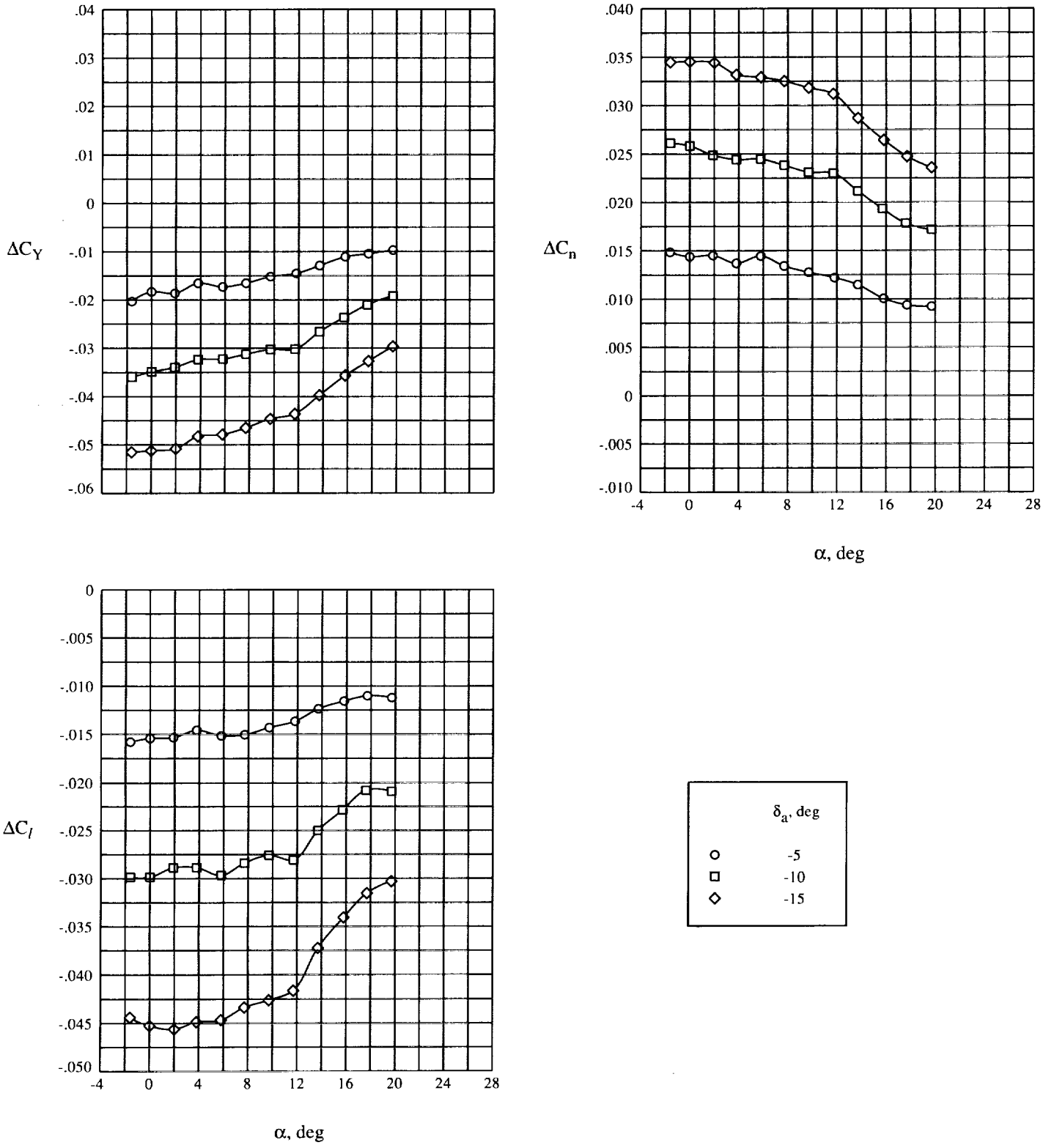

(a) Elevon deflection.

Figure 15. Roll-control effectiveness.

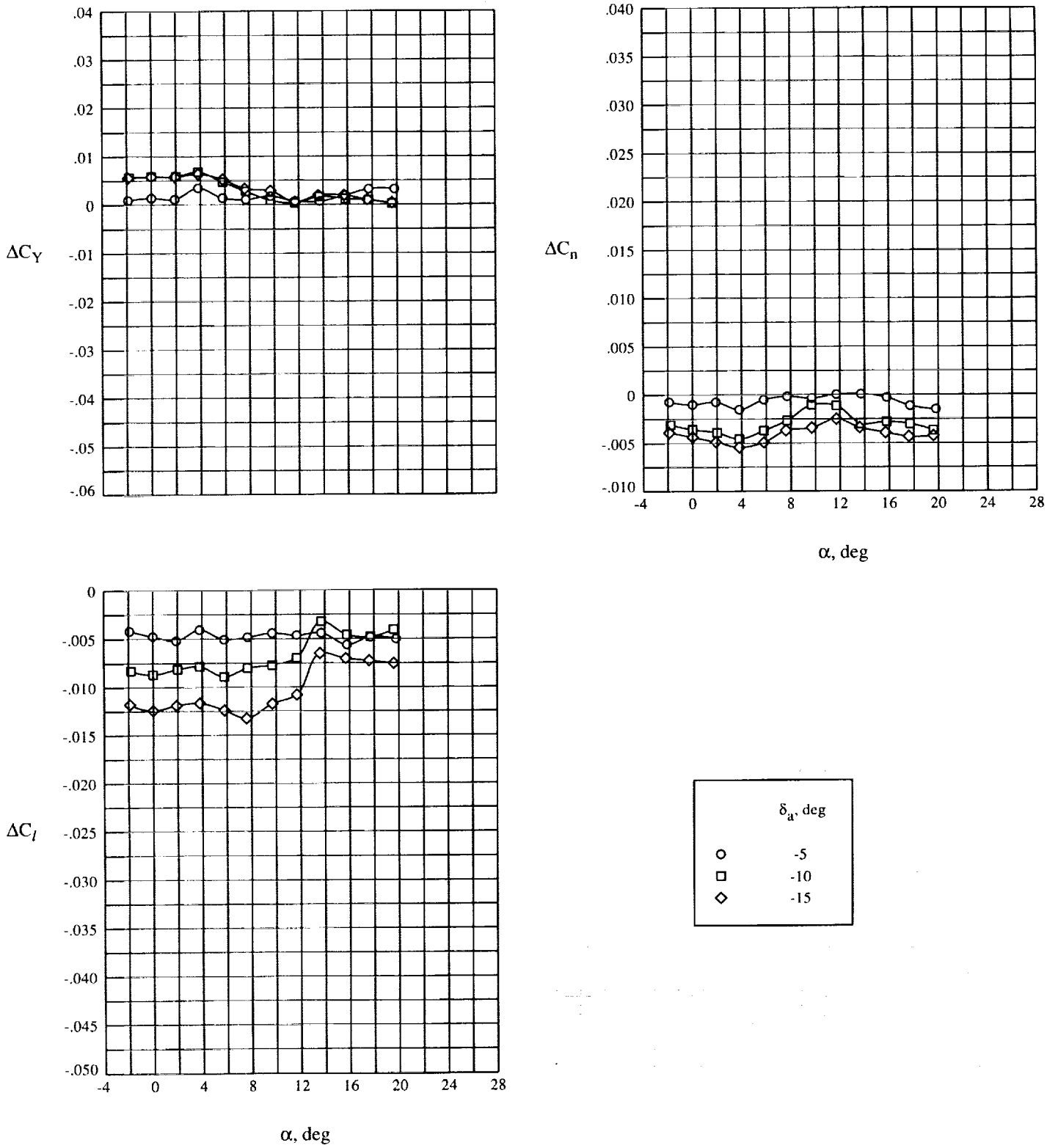

(b) Body-flap deflection.

Figure 15. Concluded.

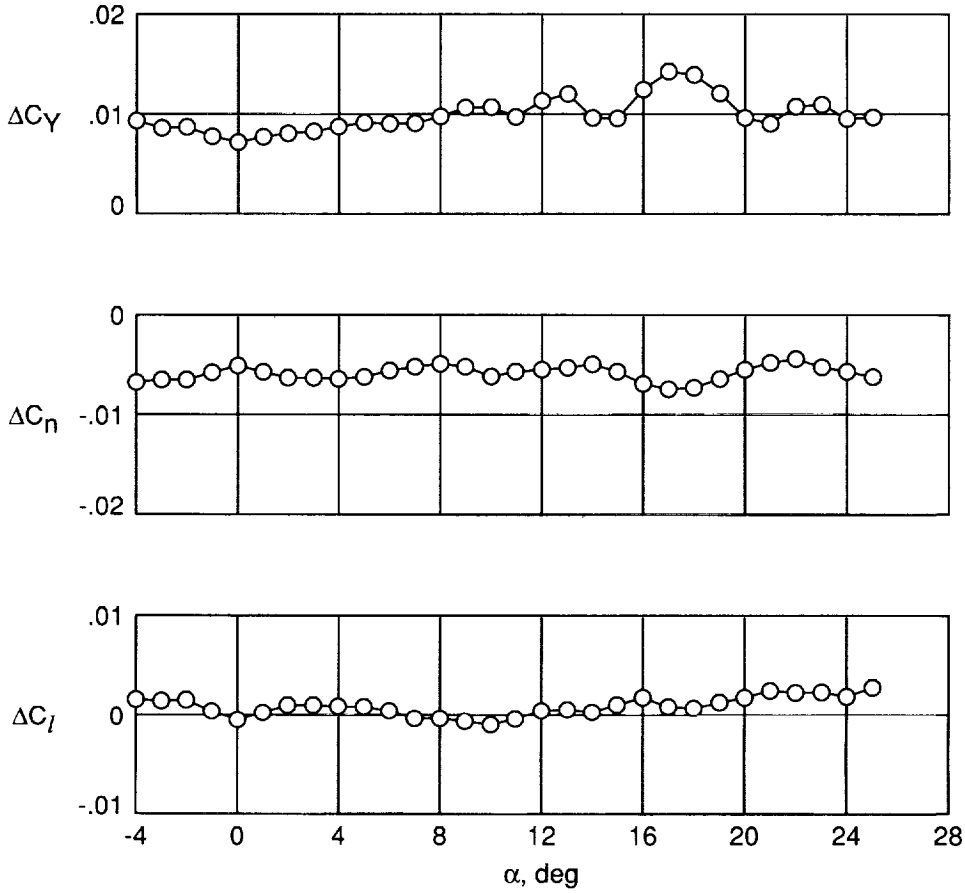

Figure 16. Yaw-control effectiveness at $\delta_r = 5°$ and $M = 0.6$. Data are taken from reference 8.

REPORT DOCUMENTATION PAGE

Form Approved
OMB No. 0704-0188

1. AGENCY USE ONLY *(Leave blank)*	2. REPORT DATE	3. REPORT TYPE AND DATES COVERED
	November 1993	Technical Memorandum

4. TITLE AND SUBTITLE
Subsonic Aerodynamic Characteristics of the HL-20 Lifting-Body Configuration

5. FUNDING NUMBERS
WU 506-40-61-01

6. AUTHOR(S)
George M. Ware and Christopher I. Cruz

7. PERFORMING ORGANIZATION NAME(S) AND ADDRESS(ES)
NASA Langley Research Center
Hampton, VA 23681-0001

8. PERFORMING ORGANIZATION REPORT NUMBER
L-17261

9. SPONSORING/MONITORING AGENCY NAME(S) AND ADDRESS(ES)
National Aeronautics and Space Administration
Washington, DC 20546-0001

10. SPONSORING/MONITORING AGENCY REPORT NUMBER
NASA TM-4515

11. SUPPLEMENTARY NOTES

12a. DISTRIBUTION/AVAILABILITY STATEMENT
Unclassified–Unlimited

Subject Categories 02 and 15

12b. DISTRIBUTION CODE

13. ABSTRACT *(Maximum 200 words)*

The HL-20 is proposed as a possible future manned spacecraft. The configuration consists of a low-aspect-ratio body with a flat undersurface. Three fins (a small centerline fin and two outboard (tip) fins set at a dihedral angle of 50°) are mounted on the aft body. The control system consists of elevon surfaces on the outboard fins, a set of four body flaps on the upper and lower aft body, and an all-movable center fin. Both the elevons and body flaps were capable of trimming the model to angles of attack from $-2°$ to above 20°. The maximum trimmed lift-drag ratio was 3.6. Replacing the flat-plate tip fins with airfoil tip fins increased the maximum trimmed lift-drag ratio to 4.2. The elevons were effective as a roll control, but they produced about as much yawing moment as rolling moment because of the tip-fin dihedral angle. The body flaps produced less rolling moment than the elevons and only small values of yawing moment. A limited investigation of the effect of varying tip-fin dihedral angle indicated that a dihedral angle of 50° was a reasonable compromise for longitudinal and lateral stability, longitudinal trim, and performance at subsonic speeds.

14. SUBJECT TERMS
Personnel Launch System (PLS); Lifting body; Spacecraft; Orbiter; Aerodynamics

15. NUMBER OF PAGES
28

16. PRICE CODE
A03

17. SECURITY CLASSIFICATION OF REPORT	18. SECURITY CLASSIFICATION OF THIS PAGE	19. SECURITY CLASSIFICATION OF ABSTRACT	20. LIMITATION OF ABSTRACT
Unclassified	Unclassified		